

Article

Experimental and Computational Evaluation of 1,2,4-Triazolium-Based Ionic Liquids for Carbon Dioxide Capture

Sulafa Abdalmageed Saadalddeen Mohammed ¹, Wan Zaireen Nisa Yahya ^{1,2,*}, Mohamad Azmi Bustam ^{1,2} and Md Golam Kibria ³

¹ Chemical Engineering Department, Universiti Teknologi PETRONAS, Seri Iskandar 32610, Perak, Malaysia; sulafa_19001261@utp.edu.my (S.A.S.M.); azmibustam@utp.edu.my (M.A.B.)

² Centre for Research in Ionic Liquid, Universiti Teknologi PETRONAS, Seri Iskandar 32610, Perak, Malaysia

³ Chemical and Petroleum Engineering, University of Calgary, 2500 University Drive NW, Calgary, AB T2N 1N4, Canada; md.kibria@ucalgary.ca

* Correspondence: zaireen.yahya@utp.edu.my; Tel.: +605-3687584

Abstract: Utilization of ionic liquids (ILs) for carbon dioxide (CO₂) capture is continuously growing, and further understanding of the factors that influence its solubility (notably for new ILs) is crucial. Herein, CO₂ absorption of two 1,2,4-triazolium-based ILs was compared with imidazolium-based ILs of different anions, namely bis(trifluoromethylsulfonyl)imide, tetrafluoroborate, and glycinate. The CO₂ absorption capacity was determined using an isochoric saturation method and compared with predicted solubility employing CONductor-like Screening Model for Real Solvents (COSMO-RS). To gain an understanding of the effects of cations and anions of the ILs on the CO₂ solubility, the molecular orbitals energy levels were calculated using TURBOMOLE. Triazolium-based ILs exhibit higher absorption capacity when compared to imidazolium-based ILs for the same anions. The results also showed that the anions' energy levels are more determinant towards solubility than the cations' energy levels, which can be explained by the higher tendency of CO₂ to accept electrons than to donate them.

Keywords: triazolium; CO₂ capture; ionic liquids; molecular interaction; COSMO-RS



check for updates

Citation: Mohammed, S.A.S.; Yahya, W.Z.N.; Bustam, M.A.; Kibria, M.G. Experimental and Computational Evaluation of 1,2,4-Triazolium-Based Ionic Liquids for Carbon Dioxide Capture. *Separations* **2023**, *10*, 192. <https://doi.org/10.3390/separations10030192>

Academic Editors: Catarina Seiça Neves, Filipa A. Vicente, Jorge Pereira and João Henrique Picado Madalena Santos

Received: 31 January 2023

Revised: 4 March 2023

Accepted: 8 March 2023

Published: 10 March 2023



Copyright: © 2023 by the authors. Licensee MDPI, Basel, Switzerland. This article is an open access article distributed under the terms and conditions of the Creative Commons Attribution (CC BY) license (<https://creativecommons.org/licenses/by/4.0/>).

1. Introduction

Carbon dioxide (CO₂) levels in the atmosphere are rising, posing a severe threat to the global climate [1–6]. Various techniques have been proposed to lower the greenhouse gas levels, like limiting industrial CO₂ emissions and lowering the use of fossil fuels [7–11]. CO₂ capture, utilization, and sequestration (CCUS) technologies are anticipated to provide an efficient industrial solution to reduce CO₂ emissions by 45% by 2050 [12–15]. The adoption of chemical processes such as adsorption, absorption, and membrane separation has been highlighted in much-reported research on carbon dioxide capture and storage technologies [13]. Moreover, technologies for low-temperature CO₂ capture, also known as cryogenic carbon capture (CCC), rely on phase changes to convert CO₂ from a gas to a liquid or solid [16]. The term “cryogenics” is mainly used to describe processes that take place at temperatures below 120 K, but frequently the term is used to describe low-temperature separation [17]. CCC has not gained much attraction due to the high cost and energy required for the process as well as the limited range of potential applications. However, many studies were performed to enhance the process [18] since it has many advantages, such as the ability to use it with a wide range of CO₂ concentrations and producing a high purity product without the use of hazardous chemicals.

Among these technologies, the most used is the absorption process with utilization of amine solvents such as monoethanolamine (MEA) and diethanolamine (DEA) [15].

Although primary and secondary amines have a high CO₂ absorption rate, they have a low absorption capacity. In addition, regeneration requires more energy due to the stability of the carbamate produced by the reaction, and high temperatures can cause several issues, such as the amine's oxidative degradation. While the bicarbonate product of tertiary amines is less stable and easier to regenerate, it also has a slower CO₂ reaction rate and less selectivity [19]. Thus, the major constraint on the amine absorption is the energy requirement due to the high enthalpy of the reaction, and the amine solvents are difficult to regenerate which results in the loss of the solvent, consequently increasing the cost of the process as well as equipment degradation due to corrosion [13]. Ionic liquids (ILs) have received attention as a potential substitute to amine solvents for CO₂ absorption and conversion media [20–26] due to their special characteristics, which include low vapor pressures, low heat capacities, liquid form over a large temperature range, and good thermal and chemical stability, as well as their corrosion inhibition properties [27–31]. Although ILs have lower CO₂ absorption capacity compared with MEA and less mass transfer due to high viscosity [32], ILs require low energy for regeneration as a result of the physical absorption mechanism. This is due to the low CO₂ sorption enthalpy (10–20 kJ/mol), which is just one-fourth of the energy used by conventional amine solutions [33]. Moreover, ILs are considered as designer solvents, which pave the way of improving CO₂ absorption capacity.

CO₂ solubility in ILs has since been the subject of a lot of research using both experimental and predictive methods [34–42]. The solubility of different gases, including carbon dioxide, was evaluated by Anthony et al. for different cations, namely imidazolium, pyrrolidinium, phosphonium, and ammonium [43]. They observed that CO₂ has strong interactions with the ILs mainly through the anions, and the maximum CO₂ solubility was found for ILs with bis(trifluoromethylsulfonyl)imide [TFSI] anion, regardless of the type of the cations. Comparably, Almantariotis et al. [44] investigated the CO₂ absorption performance using 1-alkyl-3-methylimidazolium tris(pentafluoroethyl)trifluorophosphate ILs ([C_nMIM][eFAP] with $n = 2, 4, 6$). They noticed that for the same cations, the ILs containing the highly fluorinated anions [eFAP] reported better CO₂ solubility than the [TFSI]-based ILs. Several other studies also demonstrated that the inclusion of fluoroalkyl groups in ILs increases CO₂ absorption properties [43,44].

On the other hand, amino acid based ILs have also demonstrated high CO₂ solubility [45,46]. Nooraini and Mehrdad [45] correlated the CO₂ solubility in amino acid based ILs with the molecular interactions between the amino acid anions and CO₂. Through density functional theory (DFT) simulations, they found that the N atom of the amino acid is where substantial CO₂ sorption occurs. The influence of anions, namely [TFSI], [BF₄], [methide], [NO₃], [OTf], [DCA], and [PF₆] with alkylimidazolium as the cations, was investigated by Aki et al. [47], in which they demonstrated that the CO₂ solubility marginally rises with the length of the cation's alkyl chain because longer alkyl chains have bigger free volumes and are primarily dependent on anions. The maximum CO₂ solubility was recorded for anions containing fluoroalkyl groups, such as [TFSI] and [methide], which was explained by the increase of molar volumes [47].

Furthermore, to determine the potential of ILs for separating CO₂ and H₂S gases from natural gas as well as for separating the two gases from one another in gaseous streams that contain them, Safavi and Ghotbi [48] evaluated the solubility of CO₂ and hydrogen sulfide (H₂S) in a temperatures range from 303.15 to 353.15 K and pressures up to 2 MPa in 1-octyl-3-methylimidazolium hexafluorophosphate ([C₈MIM][PF₆]). They reported that the solubility of H₂S is around three times that of CO₂ in the specific ionic liquid under study. They also highlighted that the solubility of both gases increases with increasing pressure and decreases with rising temperature. Additionally, they investigated the impact of cation alkyl chain length on the solubility of CO₂ and H₂S by comparing the experimental results with previous reported study. They deduced that the solubility of CO₂ and H₂S in the ionic liquid increases as the cation alkyl chain length increases. In addition, the influence of the anion on gas solubility was evaluated by comparing the solubility of CO₂ and H₂S

in $[\text{C}_8\text{MIM}][\text{PF}_6]$ and in $[\text{C}_8\text{MIM}][\text{TFSI}]$. They reported that both gasses CO_2 and H_2S are more soluble in the IL when $[\text{TFSI}]$ is the anion.

Further understanding of the synergistic effects of the cations, anions, alkyl chain length, and functional groups towards the molecular interactions between CO_2 and ionic liquids is of high importance. Based on the frontier molecular orbital theory, the overlap between the donor's HOMO and the acceptor's LUMO can be used to gauge how intense the donor-acceptor interactions are [49,50]. Consequently, a study of the molecular orbital energy levels' effect on CO_2 capacity is therefore relevant. Moreover, since the carbon in carbon dioxide is partially positive while the oxygen is partially negative, then there is a possibility of acid/base interaction. Hence, in this study, CO_2 absorption capacity of a series of ionic liquids of different cations, anions, and alkyl chain lengths, namely two 1,2,4-triazolium-based ILs $[\text{BBT}][\text{BF}_4]$ and $[\text{BBT}][\text{TFSI}]$, were compared with five imidazolium-based ILs, namely $[\text{EMIM}][\text{TFSI}]$, $[\text{BMIM}][\text{BF}_4]$, $[\text{HMIM}][\text{TFSI}]$, $[\text{EMIM}][\text{BF}_4]$, and $[\text{BMIM}][\text{GLY}]$. The experimental CO_2 absorption capacity for each ILs was compared with predicted values obtained from CONductor-like Screening Model for Realistic Solvents (COSMO-RS). Density functional theory (DFT) calculations were performed using TURBOMOLE to investigate the impact of the molecular orbitals of the individual (cation and anions) pairs of the ionic liquids on CO_2 absorption. The molecular structures of the seven ILs are shown in Figure 1.

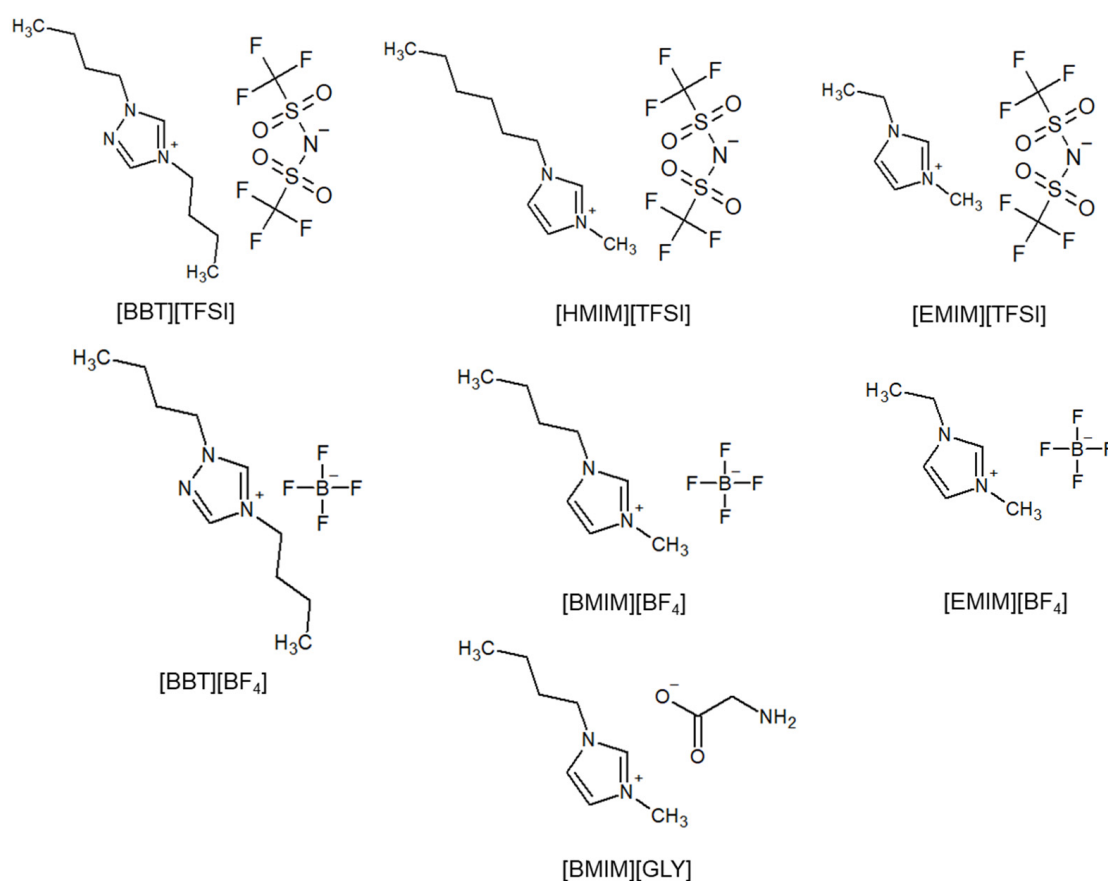


Figure 1. Molecular structures of ionic liquids used in this work.

2. Materials and Methods

2.1. Materials

In this work, the synthesis of $[\text{BBT}][\text{BF}_4]$, $[\text{BBT}][\text{TFSI}]$, $[\text{BMIM}][\text{BF}_4]$, and $[\text{BMIM}][\text{GLY}]$ was carried out in accordance with the procedures outlined in our earlier publication [51]. $[\text{EMIM}][\text{BF}_4]$ ($\geq 98.0\%$), $[\text{EMIM}][\text{TFSI}]$ ($\geq 97.0\%$), and $[\text{HMIM}][\text{TFSI}]$ ($\geq 98.0\%$) were procured from Sigma Aldrich.

2.2. Density Measurement

To aid in determination of number of moles of ILs, the density of all ILs was measured at 25 °C with an accuracy of 0.0001 g/cm³ (Stabinger Viscometer SVM3000, Anton Paar). The molar volume of the ILs was determined via Equation (1),

$$V_m = \frac{M_w}{\rho} \tag{1}$$

where M_w is the molecular weight of IL in g/mol and ρ is the density of the IL in g/cm³.

2.3. CO₂ Absorption Capacity in ILs

The isochoric saturation method to determine the CO₂ absorption capacity in the pure ILs was adapted from procedures reported in literature [52–56]. The experiments were carried out in a 15 mL capacity stainless steel high-pressure equilibrium cell (EC), as seen in Figure 2. A pressure gauge controller was attached to the system to maintain the required pressure (5 bar) and a water bath was used to maintain the cell at 25 °C.

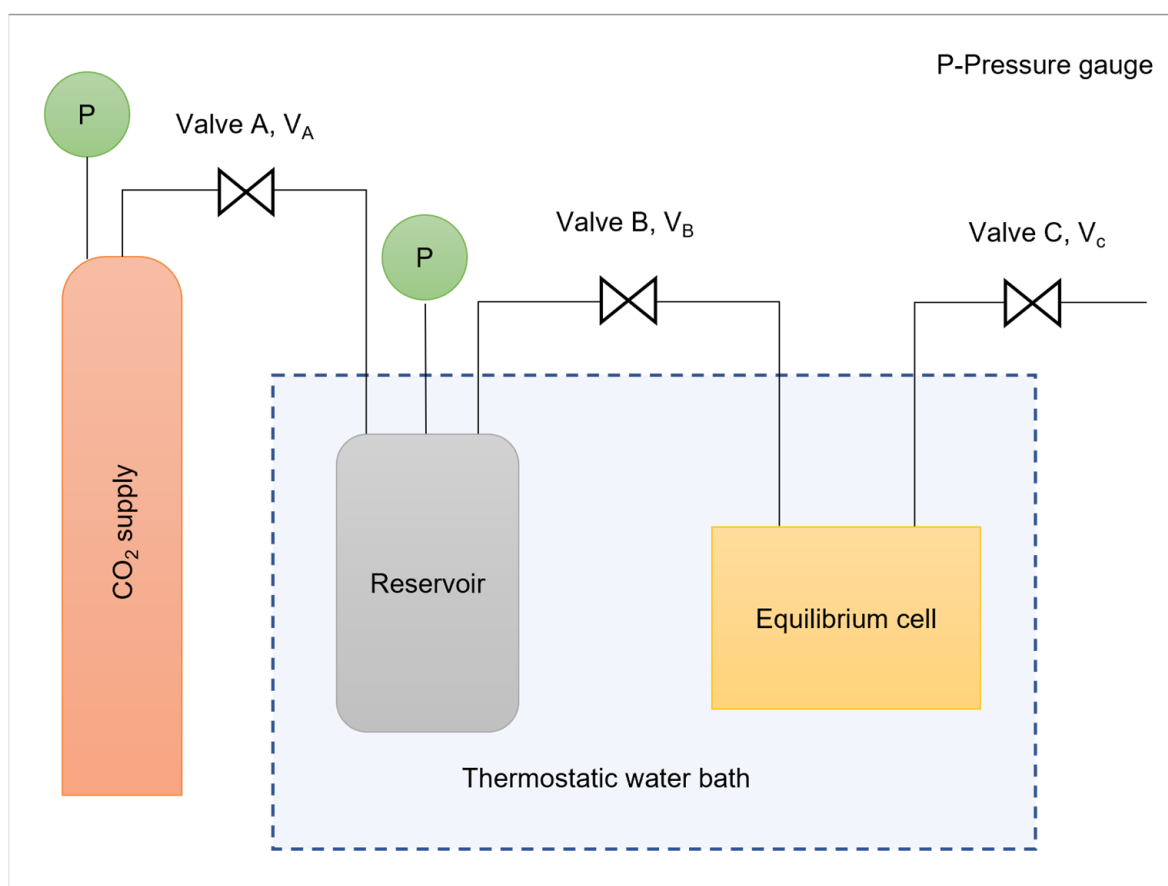


Figure 2. Schematic diagram of the isochoric saturation setup.

The IL was first loaded into the equilibrium cell during the experiment and degassed using a vacuum pump. The CO₂ gas was then supplied to the EC and the pressure inside the cell progressively dropped as the IL started to absorb CO₂. The pressure in the system was recorded every minute, and the system was given enough time to stabilize without any usage of stirrer. The time duration for reaching equilibrium varied between 160 and 200 min. The number of moles of CO₂ at the start was determined via Equation (2):

$$n_{CO_2}^i = \frac{P_i V_{res}}{Z_{CO_2}^i RT_i} \tag{2}$$

where $n_{CO_2}^i$ is the number of moles of CO₂ that were initially charged into EC, P_i is the initial pressure, V_{res} is the volume of the reservoir, $Z_{CO_2}^i$ is the compressibility factor at the starting temperature and pressure conditions, R is the universal gas constant, and T_i is the initial temperature.

Equation (3) was used to calculate the number of moles of CO₂ left inside the cell at equilibrium condition:

$$n_{CO_2}^{eq} = \frac{P_{eq}(V_{total} - V_s)}{Z_{CO_2}^f RT_{eq}} \tag{3}$$

where $n_{CO_2}^{eq}$ is the number of moles of CO₂ molecules inside the system that is at equilibrium, P_{eq} is the pressure at equilibrium, V_{total} is the volume of the CO₂ absorption system from valve A (VA) to valve C (VC), V_s is the volume of the ILs, and $Z_{CO_2}^f$ is the compressibility factor at equilibrium conditions.

Equation (4) was used to calculate the number of moles of CO₂ absorbed $n_{CO_2}^{abs}$, and the mole ratio was used to express the solubility of CO₂ (x) using Equation (5):

$$n_{CO_2}^{abs} = n_{CO_2}^i - n_{CO_2}^{eq} \tag{4}$$

$$x = \frac{n_{CO_2}^{eq}}{\frac{w_{IL}}{M_{w\ of\ IL}}} \tag{5}$$

where w_{IL} is the weight of IL and $M_{w\ of\ IL}$ is the molecular weight of IL.

2.4. Computational Methods

The molecular orbitals (HOMO-LUMO) of the individual cations and anions of the ILs were generated using TmoleX simulation software (version 4.4.1), which is a graphical user-friendly interface for the quantum chemical program package (TURBOMOLE) [8]. First the geometry optimization was performed, followed by electronic structure computations with def-TZVP basis set. To create the input file, the functional BP86 was added under the DFT setting [57,58]. COSMO-RS was used to generate the sigma profile, sigma potential, and sigma surface for the selected structures and to calculate the predicted CO₂ capacity of various ILs [59–67]. The sigma profile (σ) provides the possibility of calculating the average screening charge density on the segments of molecule (X). For solvents consisting of many components X_i , with molar concentration x_i , the σ -profile was determined by the weighted sums of the Sigma profile (σ) of the components as per Equation (6).

$$p_i(\sigma) = \sum_i^N x_i \times p_i \tag{6}$$

The σ -profile and σ -potential were categorized into three main regions: hydrogen bond donor for $\sigma < -0.01\ e/\text{\AA}^2$, the non-polar region for $-0.01 < \sigma < +0.01\ e/\text{\AA}^2$, and hydrogen bond acceptor for $\sigma > +0.01\ e/\text{\AA}^2$. Sigma surface was used to provide visual representation for charge distribution on the structure surface. Color coding was used to determine the charge distribution of the molecule: green indicates neutral nature, yellow represents a partial negative charge, blue shows the positive charge region, and the negative charge region is represented by red. The activity coefficient at infinite dilution showed the degree of non-ideal behavior in the solvents, as in Equation (7):

$$\ln(\gamma_i) = (\mu_i^{S,\infty} - \mu_i^p) / RT \tag{7}$$

where $\mu_i^{S,\infty}$ and μ_i^p are chemical potentials of both solvent and pure compounds, respectively. The inverse activity coefficient of a solute i , obtained at infinite dilution of the solute in the IL solvent ($\gamma_i^{IL,\infty}$), was used to describe a solute's capacity solubility capacity C_i^{IL} in an IL solvent as in Equation (8).

$$C_i^{IL} = 1/\gamma_i^{IL,\infty} \tag{8}$$

The IL capacity C_i^{IL} thus corresponds to a non-iterative and unnormalized liquid solubility of solute i in the IL in mole fraction units [mol_{*i*}/mol_{IL}]. The IL stoichiometry scales the IL capacity calculated by COSMO-RS. On the other hand, the IL capacity can be defined in mass-based units as per Equation (9).

$$G_i^{IL} = MW_i / (MW_{IL} \gamma_i^{IL,\infty}) \quad (9)$$

The non-iterative and unnormalized mass-based liquid solubility of solute i in the IL is represented by the IL capacity with units [g_{*i*}/g_{IL}]. C_i^{IL} and G_i^{IL} are semi-quantitative relative measurements of how efficiently an IL solvent dissolves a certain solute i . Therefore, the IL capacity can be used to compare the solubility properties of several IL solvents for a specific solute [68]. The COSMO-RS theory is well illustrated elsewhere by the developer [69–71]. The sigma profile, sigma potential, and sigma surface are available in the supporting information.

3. Results and Discussions

3.1. Density and CO₂ Solubility of Different ILs

The density, the calculated molar volumes, and the maximum CO₂ absorption capacity of the selected ILs measured at 25 °C are shown in Table 1 and the CO₂ capacity of ILs vs. time depicted in Figure 3. The [TFSI]-based ILs with large anions exhibit the highest density and molar volumes compared to other types of anions. Interestingly, the triazolium-based ILs exhibit lower density than the imidazolium ILs for the same anions. This is favorable to allow more carbon dioxide to be absorbed in the ILs as the gas solubility is known to be dependent on the molar volume of the ILs where the CO₂ will occupy the free space between the ions [18,20,42].

Table 1. The density at 25 °C, the molar volume, and the maximum capacity values for different ILs.

| Ionic Liquids | Density (g/cm ³) | Molecular Weight, MW (g/mol) | Molar Volume (cm ³ /mol) | Maximum Capacity Values, x_r (Mol (CO ₂ abs)/Mol (IL)) |
|--------------------------|------------------------------|------------------------------|-------------------------------------|---|
| [EMIM][BF ₄] | 1.280 | 197.97 | 154.63 | 0.0795 |
| [BMIM][BF ₄] | 1.222 | 226.02 | 185.03 | 0.0972 |
| [BMIM][GLY] | 1.108 | 213.29 | 192.48 | 0.2150 |
| [BBT][BF ₄] | 1.154 | 269.09 | 233.12 | 0.1553 |
| [EMIM][TFSI] | 1.517 | 391.3 | 257.96 | 0.1808 |
| [HMIM][TFSI] | 1.371 | 447.42 | 326.35 | 0.2335 |
| [BBT][TFSI] | 1.359 | 462.45 | 340.19 | 0.2523 |

From the results shown in Table 1 and Figure 3, it can be observed that the order of CO₂ capacity in ILs starting from the highest is [BBT][TFSI] > [HMIM][TFSI] > [BMIM][GLY] > [EMIM][TFSI] > [BBT][BF₄] > [BMIM][BF₄] > [EMIM][BF₄]. The triazolium-based ILs recorded high CO₂ absorption capacity compared to the imidazolium-based ILs, with the results of the latter consistent with other reported data [43,72–75]. It can be seen that the higher the molar volumes, the higher the absorption capacity, except for the case of [BMIM][GLY]. The absorption mechanism can be classified either by physisorption or chemisorption, with the latter being governed by a rate-limiting process but resulting in higher absorption capacity [76]. This can be seen in [BMIM][GLY], where a sharp increase of CO₂ absorption is observed until it stabilizes to its maximum capacity, which can be classified to follow the chemisorption process. On the other hand, in the case of physisorption, the CO₂ solubility depends on the fractional free volume of the ILs, which explains the good solubility of the large delocalized anions [TFSI] compared to [BF₄] [77]. Further investigations were performed to determine the factors that influence

the absorption types in ionic liquids, and parameters such as the type of cations, anions, and the alkyl chain length were taken into consideration.

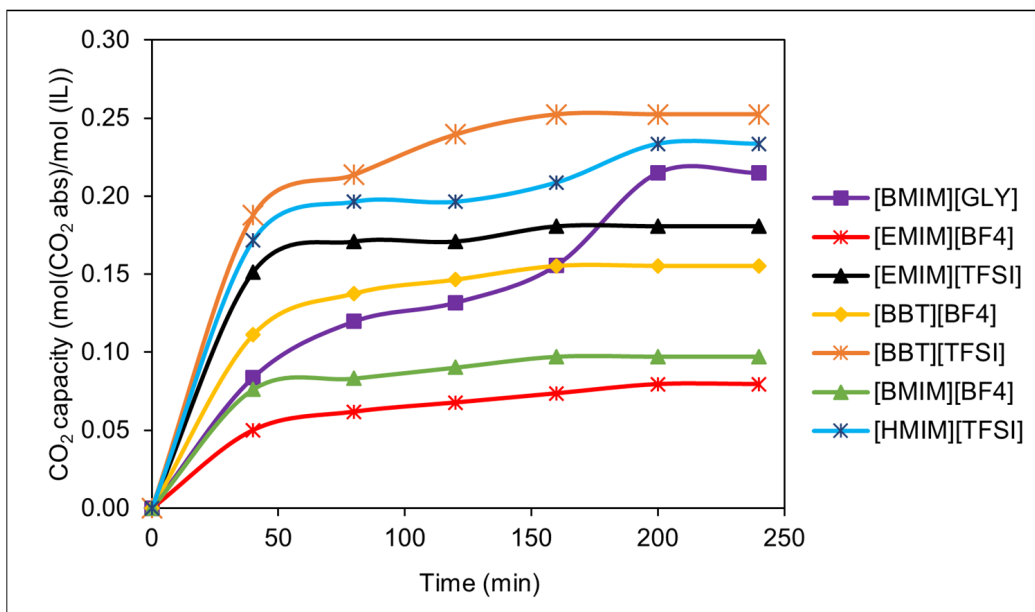


Figure 3. The amount of mole CO₂ absorbed/mole IL.

Figure 4 depicts the CO₂ capacity for different ILs through experimental and computational methods using COSMO-RS. By comparing the two methods, a linear regression ($y = 11.381x + 0.9218$) was obtained with R-squared value of 0.9374. It is noteworthy to highlight that the values from COSMO-RS are larger than the experimental results because COSMO-RS is a qualitative tool, and the capacity values are computed by employing the infinite dilution activity coefficients of the ILs. The COSMO-RS is therefore an effective tool for estimation of thermodynamic properties and reliable for prediction of gas solubility properties for new ionic liquids.

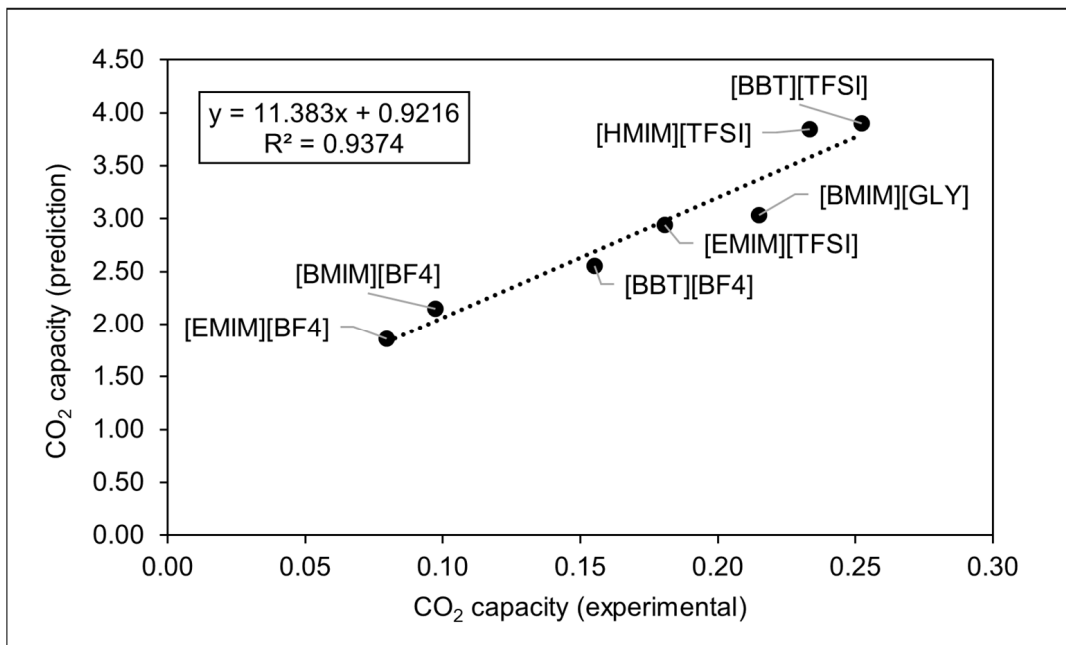


Figure 4. Quantitative comparison between experimental and computational CO₂ capacity.

3.2. Role of the Anions on the ILs' Capacity to Dissolve CO₂

To investigate the role of anions on CO₂ solubility in IL, a comparison of the CO₂ capacity values for [BBT][BF₄], [BBT][TFSI], [BMIM][BF₄], and [BMIM][GLY] was performed. It is apparent from Figure 3 that [BBT][BF₄] shows less capacity of CO₂ as compared to [BBT][TFSI], while [BMIM][GLY] has a higher CO₂ solubility than [BMIM][BF₄]. As reported by Aki et al., the solubility of CO₂ is not only determined by the acid/base interactions between CO₂ and the anions; they give the example of the basicity of [BF₄] which is reported experimentally higher than [TFSI], which eventually should show higher absorption capacity [47]. To understand this conflicting result, it is worth highlighting that there are three primary theories of acid–base, namely the Arrhenius theory (acid is a substance that produces H⁺ ions in water and base is a substance that produces OH⁻ ions in water), the Bronsted–Lowry theory (acid is a proton H⁺ donor and a base is a proton H⁺ acceptor), and lastly the Lewis acid–base theory (acid is an electron pair acceptor and base is an electron pair donor). The Lewis acid–base describes the bonding in quite different compounds, unlike the Bronsted acid–base concept, and thus can better explain the CO₂–ILs interaction [78]. Onofri et al. suggested that the glycinate anion reacted with CO₂ by two-step mechanisms involving an initial nucleophilic attack followed by a proton transfer process [76].

The interaction of the ionic liquids and the CO₂ can be further elucidated using the frontier molecular orbital theory [49,50]. We stipulated that the ionic liquids and CO₂ interaction can be explained by the donation of electrons from the HOMO level of the anions of the ionic liquids into the LUMO level of CO₂. Hence, to confirm this theory, the LUMO and the HOMO for the anions were calculated using Tmolex, as shown in Figure 5. Here, it can be observed that the [TFSI] anion has a higher HOMO value compared to the [BF₄] anion. It can be deduced that an increment in the HOMO values of anions increases the capacity of CO₂ in ILs. Alternately, the sigma profiles of [TFSI] and [BF₄] (cf. Figures S1 and S2) were evaluated to provide insight into the hydrogen bonding strength. The sigma profiles reveal that the [TFSI] anion is a greater hydrogen bond acceptor than [BF₄]. This results in a higher tendency for the [TFSI] anion to donate electrons compared to [BF₄].

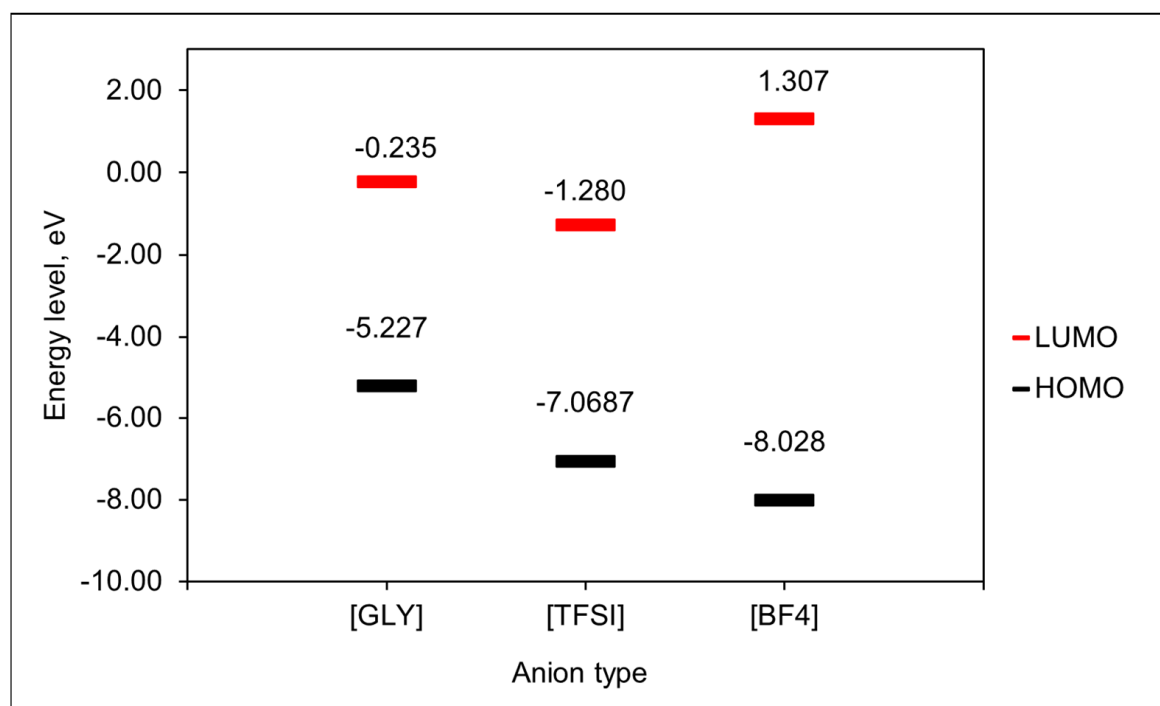


Figure 5. Values of HOMO-LUMO for [GLY], [BF₄], and [TFSI] anions.

Further comparison was made between [BMIM][BF₄] and [BMIM][GLY], whereby [BMIM][GLY] has shown a higher CO₂ solubility than [BMIM][BF₄]. From the HOMO–LUMO energy levels for anions, as shown in Figure 5, it can be observed that glycinate has a higher HOMO value. The results are also consistent with previous studies, which reported the order of CO₂ solubility starting from the highest is [BMIM][GLY] > [BMIM][TFSI] > [BMIM][BF₄] [43,73–75]. It can be noted that the order of CO₂ capacity is the same as the HOMO energy levels starting from the highest. It can be concluded that the anions that have higher HOMO energy levels show good CO₂ capacity since CO₂ in this case is considered as the Lewis acid and the anions are considered as the Lewis base, which means the gap between the HOMO of anion and the LUMO of CO₂ will be the lowest for the case of [BMIM][GLY]. This is also aligned with the sigma profiles and sigma potential, as shown in Figures S3 and S4, respectively, where [GLY] has a higher tendency to donate electrons compared to [BF₄]. Moreover, it can be noted that the good absorption in [BMIM][GLY] is due to the special characteristic of [GLY], which has a very high HOMO value as well as the terminal electronegatively charged which can be observed from the sigma surface in Figure S13. These two parameters could be the reason for the strong interaction that leads to chemisorption. Unlike other anions, such as [BF₄] which has relatively low HOMO values and also unlike [TFSI] which has a relatively high HOMO value, due to the big structure and the charge distribution as shown in the sigma surface in Figure S13, the interaction is not as strong which led to physisorption rather than by chemisorption.

3.3. Role of the Cations on the ILs' Capacity to Dissolve CO₂

On the other hand, to investigate the impact of cations on CO₂ absorption in ILs, the CO₂ capacity values for [BBT][BF₄], [BMIM][BF₄], and [EMIM][BF₄] are compared, while Figure 6 displays the HOMO–LUMO energy levels of the cations.

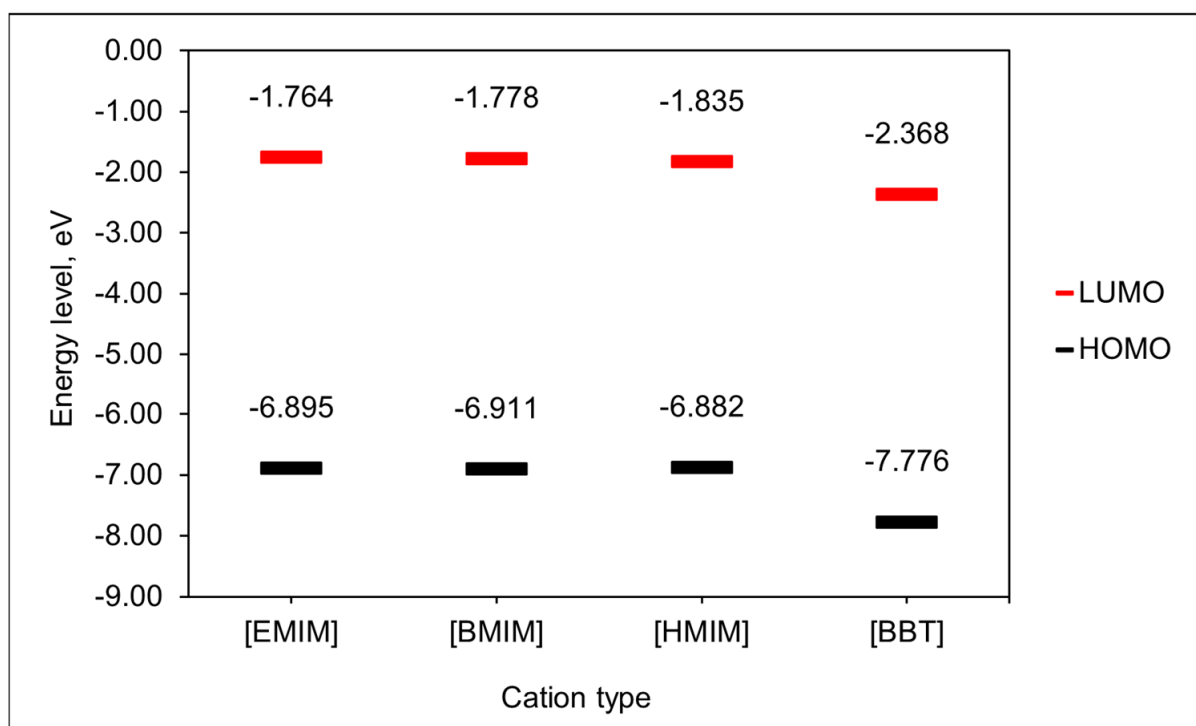


Figure 6. HOMO–LUMO energy levels for different cations.

The order of CO₂ capacity, starting from the highest, is [BBT][BF₄] > [BMIM][BF₄] > [EMIM][BF₄] as depicted in Figure 3. From Figure 6, the LUMO values of cations starting from the lowest is [BBT] < [BMIM] < [EMIM]. It can then be inferred that the cations with lower LUMO energy levels have higher CO₂ capacity. Furthermore, based on the sigma

profiles and sigma potentials in Figures S5 and S6, it can be noted that the [BBT] cation has a higher tendency to accept electrons, followed by [BMIM] and then [EMIM].

To further validate this assumption, another comparison between CO₂ capacity for [EMIM][TFSI], [HMIM][TFSI], and [BBT][TFSI] is carried out. From Figure 3, the order of CO₂ capacity starting from the highest is [BBT][TFSI] > [HMIM][TFSI] > [EMIM][TFSI]. A similar trend is observed in terms of LUMO energy levels of cations starting from the lowest, which is [BBT] < [HMIM] < [EMIM], as displayed in Figure 6.

From these results, we observed that the cations with lower LUMO values have higher CO₂ capacity. Kong et al. reported that CO₂ can act as an acid or base according to the surrounding condition [79]. In this case, CO₂ is considered a Lewis base, and the cations are considered a Lewis acid. The sigma profiles and sigma potentials (Figures S7 and S8) also confirm that the triazolium cation has a higher tendency to accept electrons, followed by [HMIM] and then [EMIM].

3.4. Effect of the Alkyl Chain Length on CO₂ Solubility of the ILs

To study the effect of cation's alkyl chain length on CO₂ solubility in ILs, and to further validate previously reported studies, CO₂ capacity values of [BMIM][BF₄] and [EMIM][BF₄] were evaluated. From Figure 3, it can be noted that more CO₂ can be dissolved in [BMIM][BF₄] of a higher alkyl chain as compared to [EMIM][BF₄]. Similarly, [BMIM] (C₄) has a slightly lower LUMO value as compared to [EMIM] (C₂), as shown in Figure 6. Their sigma profiles and sigma potentials (Figures S9 and S10) also show that [BMIM] has a slightly higher tendency to accept electrons compared to [EMIM].

Similarly, in another comparison between CO₂ capacity for [EMIM][TFSI] and [HMIM][TFSI] it can be noted that CO₂ is more soluble in [HMIM][TFSI] as compared to [EMIM][TFSI], which correlates with a lower LUMO energy level for [HMIM] (C₆) as compared to [EMIM] (C₂), as shown in Figure 6. From the sigma profiles and sigma potentials (Figures S11 and S12), it can be observed that [HMIM] has a higher tendency to accept electrons compared to [EMIM].

The results are aligned with other reported studies, whereby the CO₂ solubility marginally improves by the increase of the cation's alkyl chain length because the longer alkyl chains in ILs have a bigger free volume [47]. Based on our study, it is noteworthy to mention that the enhancement in CO₂ solubility when the alkyl chain length increases is due to the lower LUMO energy level of the cations that have a longer alkyl chain. Furthermore, by analyzing the experimental and theoretical CO₂ capacity of the ILs and the HOMO-LUMO energy levels, it can be deduced that the anions have more influence on the solubility compared to cations, thus the HOMO energy level of the anion is more determinant than the LUMO energy level of the cation. This can be described by the fact that CO₂ tends to receive electrons more often than to donate them. It can be concluded that to have good CO₂ solubility, it is recommended for the combination of ILs to use a cation of low LUMO energy level and an anion of high HOMO energy level.

4. Conclusions

In this study, the triazolium-based ionic liquids demonstrated higher solubility of CO₂ when compared with imidazolium-based ILs of different anions. As a result of our investigation into the CO₂ capacity of ILs using experimental and computational methods, we demonstrated that the increase of HOMO energy levels of the anions and the decrease of LUMO energy levels of the cations boost the CO₂'s loading capacity in ILs. Moreover, it was also noted that the anion's HOMO energy level has a greater impact on solubility than the cation's LUMO energy level, which can be explained by the fact that CO₂ tends to receive electrons more often than to donate them. Furthermore, it was shown that as the length of the cation's alkyl chain increases, the cation's LUMO energy level decreases, thus increasing the CO₂ solubility. The results obtained can aid in selecting suitable combinations of cation-anion pairs of ILs for CO₂ absorption.

Supplementary Materials: The following supporting information can be downloaded at: <https://www.mdpi.com/article/10.3390/separations10030192/s1>. Figure S1: Sigma profile for TFSI and BF₄; Figure S2: Sigma potential for TFSI and BF₄; Figure S3: Sigma profile for GLY and BF₄; Figure S4: Sigma potential for GLY and BF₄; Figure S5: Sigma profiles for EMIM, BMIM, BBT, and BF₄; Figure S7: Sigma profiles for EMIM, HMIM, BBT, and TFSI; Figure S8: Sigma potentials for EMIM, HMIM, BBT, and TFSI; Figure S9: Sigma profiles for EMIM and BMIM (zoom); Figure S10: Sigma potentials for EMIM and BMIM; Figure S11: Sigma profiles for EMIM, HMIM and TFSI; Figure S12: Sigma potentials for EMIM, HMIM and TFSI; Figure S13: Sigma surface for the chosen cations and anions by employing COSMO-RS. Ref. [80] are cited in the Supplementary Materials.

Author Contributions: S.A.S.M.: Visualization, Investigation, Writing—Original draft preparation. W.Z.N.Y.: Conceptualization, Writing—Review and Editing, Supervision, Funding acquisition. M.A.B.: Supervision, Resources. M.G.K.: Supervision. All authors have read and agreed to the published version of the manuscript.

Funding: This work is financially supported under the Ministry of Higher Education of Malaysia Fundamental Research Grant Scheme initiative (MOHE-FRGS/1/2021/TK0/UTP/02/12).

Data Availability Statement: All data have been presented in the paper and in Supplementary Materials.

Acknowledgments: The Chemical Engineering Department and the Centre of Research in Ionic Liquids of Universiti Teknologi PETRONAS are acknowledged for providing technical assistance and research facilities.

Conflicts of Interest: The authors declare no conflict of interest.

References

1. Shama, V.M.; Swami, A.R.; Aniruddha, R.; Sreedhar, I.; Reddy, B.M. Process and engineering aspects of carbon capture by ionic liquids. *J. CO₂ Util.* **2021**, *48*, 101507. [[CrossRef](#)]
2. Cassia, R.; Nocioni, M.; Correa-Aragunde, N.; Lamattina, L. Climate Change and the Impact of Greenhouse Gases: CO₂ and NO_x, Friends and Foes of Plant Oxidative Stress. *Front. Plant Sci.* **2018**, *9*, 273. [[CrossRef](#)] [[PubMed](#)]
3. Friedlingstein, P.; Jones, M.W.; O'Sullivan, M.; Andrew, R.M.; Bakker, D.C.E.; Hauck, J.; Le Quééré, C.; Peters, G.P.; Peters, W.; Pongratz, J. Global carbon budget 2021. *Earth Syst. Sci. Data* **2022**, *14*, 1917–2005. [[CrossRef](#)]
4. Franta, B. Early oil industry knowledge of CO₂ and global warming. *Nat. Clim. Chang.* **2018**, *8*, 1024–1025. [[CrossRef](#)]
5. Baker, H.S.; Millar, R.J.; Karoly, D.J.; Beyerle, U.; Guillod, B.P.; Mitchell, D.; Shiogama, H.; Sparrow, S.; Woollings, T.; Allen, M.R. Higher CO₂ concentrations increase extreme event risk in a 1.5 °C world. *Nat. Clim. Chang.* **2018**, *8*, 604–608. [[CrossRef](#)]
6. Dey, S.; Dhal, G.C. Materials Science for Energy Technologies. *Mater. Sci. Technol.* **2019**, *2*, 607–623.
7. Markewitz, P.; Kuckshinrichs, W.; Leitner, W.; Linsen, J.; Zapp, P.; Bongartz, R.; Schreiber, A.; Müller, T.E. Worldwide innovations in the development of carbon capture technologies and the utilization of CO₂. *Energy Environ. Sci.* **2012**, *5*, 7281–7305. [[CrossRef](#)]
8. Sinha, R.K.; Chaturvedi, N.D. A review on carbon emission reduction in industries and planning emission limits. *Renew. Sustain. Energy Rev.* **2019**, *114*, 109304. [[CrossRef](#)]
9. Peter, S.C. Reduction of CO₂ to Chemicals and Fuels: A Solution to Global Warming and Energy Crisis. *ACS Energy Lett.* **2018**, *3*, 1557–1561. [[CrossRef](#)]
10. Benhelal, E.; Shamsaei, E.; Rashid, M.I. Challenges against CO₂ abatement strategies in cement industry: A review. *J. Environ. Sci.* **2021**, *104*, 84–101. [[CrossRef](#)]
11. Gür, T.M. Carbon dioxide emissions, capture, storage and utilization: Review of materials, processes and technologies. *Prog. Energy Combust. Sci.* **2022**, *89*, 100965. [[CrossRef](#)]
12. Langevin, J.; Harris, C.B.; Reyna, J.L. Assessing the potential to reduce US building CO₂ emissions 80% by 2050. *Joule* **2019**, *3*, 2403–2424. [[CrossRef](#)]
13. Hong, W.Y. A techno-economic review on carbon capture, utilisation and storage systems for achieving a net-zero CO₂ emissions future. *Carbon Capture Sci. Technol.* **2022**, *3*, 100044. [[CrossRef](#)]
14. Zhang, L.; Sun, N.; Wang, M.; Wu, T.; Wei, W.; Pang, C.H. The integration of hydrogenation and carbon capture utilisation and storage technology: A potential low-carbon approach to chemical synthesis in China. *Int. J. Energy Res.* **2021**, *45*, 19789–19818. [[CrossRef](#)]
15. Ghiat, I.; Al-Ansari, T. A review of carbon capture and utilisation as a CO₂ abatement opportunity within the EWF nexus. *J. CO₂ Util.* **2021**, *45*, 101432. [[CrossRef](#)]
16. Berstad, D.; Anantharaman, R.; Neksa, P. Low-temperature CO₂ capture technologies—Applications and potential. *Int. J. Refrig.* **2013**, *36*, 1403–1416. [[CrossRef](#)]
17. Timmerhaus, K.D.; Reed, R.P. *Cryogenic Engineering: Fifty Years of Progress*; Springer: New York, NY, USA, 2007.
18. Font-Palma, C.; Cann, D.; Udemu, C. Review of cryogenic carbon capture innovations and their potential applications. *C* **2021**, *7*, 58. [[CrossRef](#)]

19. Meng, F.; Meng, Y.; Ju, T.; Han, S.; Lin, L.; Jiang, J. Research progress of aqueous amine solution for CO₂ capture: A review. *Renew. Sustain. Energy Rev.* **2022**, *168*, 112902. [[CrossRef](#)]
20. Muldoon, M.J.; Aki, S.N.; Anderson, J.L.; Dixon, J.K.; Brennecke, J.F. Improving carbon dioxide solubility in ionic liquids. *J. Phys. Chem. B* **2007**, *111*, 9001–9009. [[CrossRef](#)]
21. Sun, Y.; Schemann, A.; Held, C.; Lu, X.; Shen, G.; Ji, X. Modeling thermodynamic derivative properties and gas solubility of ionic liquids with ePC-SAFT. *Ind. Eng. Chem. Res.* **2019**, *58*, 8401–8417. [[CrossRef](#)]
22. Debski, B.; Hänel, A.; Aranowski, R.; Stolte, S.; Markiewicz, M.; Veltzke, T.; Cichowska-Kopczyńska, I. Thermodynamic interpretation and prediction of CO₂ solubility in imidazolium ionic liquids based on regular solution theory. *J. Mol. Liq.* **2019**, *291*, 110477. [[CrossRef](#)]
23. Moosanezhad-Kermani, H.; Rezaei, F.; Hemmati-Sarapardeh, A.; Band, S.S.; Mosavi, A. Modeling of carbon dioxide solubility in ionic liquids based on group method of data handling. *Eng. Appl. Comput. Fluid Mech.* **2021**, *15*, 23–42. [[CrossRef](#)]
24. Aghaie, M.; Rezaei, N. A systematic review on CO₂ capture with ionic liquids: Current status and future prospects. *Renew. Sustain. Energy Rev.* **2018**, *96*, 502–525. [[CrossRef](#)]
25. Lu, J.G.; Li, X.; Zhao, Y.X.; Ma, H.L.; Wang, L.F.; Wang, X.Y.; Yu, Y.F.; Shen, T.Y.; Xu, H.; Zhang, Y.T. CO₂ capture by ionic liquid membrane absorption for reduction of emissions of greenhouse gas. *Environ. Chem. Lett.* **2019**, *17*, 1031–1038. [[CrossRef](#)]
26. Hospital-Benito, D.; Lemus, J.; Moya, C.; Santiago, R.; Palomar, J. Process analysis overview of ionic liquids on CO₂ chemical capture. *Chem. Eng. J.* **2020**, *390*, 124509. [[CrossRef](#)]
27. Ghandi, K. A review of ionic liquids, their limits and applications. *Green Sustain. Chem.* **2014**, *4*, 44–53. [[CrossRef](#)]
28. Zhang, W.; Gao, E.; Li, Y.; Bernardis, M.T.; He, Y.; Shi, Y. CO₂ capture with polyamine-based protic ionic liquid functionalized mesoporous silica. *J. CO₂ Util.* **2019**, *34*, 606–615. [[CrossRef](#)]
29. Xue, Z.; Qin, L.; Jiang, J.; Mu, T.; Gao, G. Thermal, electrochemical and radiolytic stabilities of ionic liquids. *Phys. Chem. Chem. Phys.* **2018**, *20*, 8382–8402. [[CrossRef](#)]
30. Verma, C.; Ebenso, E.E.; Quraishi, M.A. Ionic liquids as green and sustainable corrosion inhibitors for metals and alloys: An overview. *J. Mol. Liq.* **2017**, *233*, 403–414. [[CrossRef](#)]
31. Wang, S.; Li, Z.; Zhang, Y.; Liu, X.; Han, J.; Li, X.; Liu, Z.; Liu, S.; Choy, W.C. Water-soluble triazolium ionic-liquid-induced surface self-assembly to enhance the stability and efficiency of perovskite solar cells. *Adv. Funct. Mater.* **2019**, *29*, 1900417. [[CrossRef](#)]
32. Aghel, B.; Janati, S.; Wongwiset, S.; Shadloo, M.S. Review on CO₂ capture by blended amine solutions. *Int. J. Greenh. Gas Control* **2022**, *119*, 103715. [[CrossRef](#)]
33. Solangi, N.H.; Hussin, F.; Anjum, A.; Sabzoi, N.; Mazari, S.A.; Mubarak, N.M.; Aroua, M.K.; Siddiqui, M.T.H.; Qureshi, S.S. A review of encapsulated ionic liquids for CO₂ capture. *J. Mol. Liq.* **2023**, *374*, 121266. [[CrossRef](#)]
34. Neumann, J.G.; Stassen, H. Anion effect on gas absorption in imidazolium-based ionic liquids. *J. Chem. Inf. Model.* **2020**, *60*, 661–666. [[CrossRef](#)]
35. Zhao, Z.; Huang, Y.; Zhang, Z.; Fei, W.; Luo, M.; Zhao, Y. Experimental and simulation study of CO₂ and H₂S solubility in propylene carbonate, imidazolium-based ionic liquids and their mixtures. *J. Chem. Thermodyn.* **2020**, *142*, 106017. [[CrossRef](#)]
36. Yim, J.H.; Park, K.W.; Oh, B.K.; Lim, J.S. CO₂ Solubility in 1,1,2,2-Tetrafluoroethanesulfonate Anion-Based Ionic Liquids: [EMIM][TFES], [BMIM][TFES], and [BNMIM][TFES]. *J. Chem. Eng. Data* **2020**, *65*, 617–627. [[CrossRef](#)]
37. Darabi, M.; Pahlavanzadeh, H. Mathematical modeling of CO₂ membrane absorption system using ionic liquid solutions. *Chem. Eng. Process.* **2020**, *147*, 107743. [[CrossRef](#)]
38. Huang, Q.; Jing, G.; Zhou, X.; Lv, B.; Zhou, Z. A novel biphasic solvent of amino-functionalized ionic liquid for CO₂ capture: High efficiency and regenerability. *J. CO₂ Util.* **2018**, *25*, 22–30. [[CrossRef](#)]
39. Song, Z.; Shi, H.; Zhang, X.; Zhou, T. Prediction of CO₂ solubility in ionic liquids using machine learning methods. *Chem. Eng. Sci.* **2020**, *223*, 115752. [[CrossRef](#)]
40. Venkatraman, V.; Alsberg, B.K. Predicting CO₂ capture of ionic liquids using machine learning. *J. CO₂ Util.* **2017**, *21*, 162–168. [[CrossRef](#)]
41. Dashti, A.; Harami, H.R.; Rezakazemi, M.; Shirazian, S. Estimating CH₄ and CO₂ solubilities in ionic liquids using computational intelligence approaches. *J. Mol. Liq.* **2018**, *271*, 661–669. [[CrossRef](#)]
42. Jiang, W.; Li, X.; Gao, G.; Wu, F.; Luo, C.; Zhang, L. Advances in applications of ionic liquids for phase change CO₂ capture. *Chem. Eng. J.* **2022**, *445*, 136767. [[CrossRef](#)]
43. Anthony, J.L.; Anderson, J.L.; Maginn, E.J.; Brennecke, J.F. Anion effects on gas solubility in ionic liquids. *J. Phys. Chem. B* **2005**, *109*, 6366–6374. [[CrossRef](#)] [[PubMed](#)]
44. Almantariotis, D.; Stevanovic, S.; Fandino, O.; Pensado, A.S.; Padua, A.A.; Coxam, J.Y.; Costa Gomes, M.F. Absorption of Carbon Dioxide, Nitrous Oxide, Ethane and Nitrogen by 1-Alkyl-3-methylimidazolium (Cnmim, n = 2,4,6) Tris(pentafluoroethyl)trifluorophosphate Ionic Liquids (eFAP). *J. Phys. Chem. B* **2012**, *116*, 7728–7738. [[CrossRef](#)] [[PubMed](#)]
45. Noorani, N.; Mehrdad, A. CO₂ solubility in some amino acid-based ionic liquids: Measurement, correlation and DFT studies. *Fluid Phase Equilib.* **2020**, *517*, 112591. [[CrossRef](#)]
46. Wei, L.; Guo, R.; Tang, Y.; Zhu, J.; Liu, M.; Chen, J.; Xu, Y. Properties of aqueous amine based protic ionic liquids and its application for CO₂ quick capture. *Sep. Purif. Technol.* **2020**, *239*, 116531. [[CrossRef](#)]
47. Aki, S.N.; Mellein, B.R.; Saurer, E.M.; Brennecke, J.F. High-pressure phase behavior of carbon dioxide with imidazolium-based ionic liquids. *J. Phys. Chem. B* **2004**, *108*, 20355–20365. [[CrossRef](#)]

48. Safavi, M.; Ghotbi, C.; Taghikhani, V.; Jalili, A.H.; Mehdizadeh, A. Study of the solubility of CO₂, H₂S and their mixture in the ionic liquid 1-octyl-3-methylimidazolium hexafluorophosphate: Experimental and modelling. *J. Chem. Thermodyn.* **2013**, *65*, 220–232. [[CrossRef](#)]
49. Fukui, K. *Theory of Orientation and Stereoselection*; Springer: Berlin/Heidelberg, Germany, 1975.
50. Liu, C.; Li, Y.; Takao, M.; Toyao, T.; Maeno, Z.; Kamachi, T.; Hinuma, Y.; Takigawa, I.; Shimizu, K.I. Frontier molecular orbital based analysis of solid–adsorbate interactions over group 13 metal oxide surfaces. *J. Phys. Chem. C* **2020**, *124*, 15355–15365. [[CrossRef](#)]
51. Mohammed, S.A.S.; Yahya, W.Z.N.; Bustam, M.A.; Kibria, M.G.; Masri, A.N.; Kamonwel, N.D.M. Study of the ionic liquids' electrochemical reduction using experimental and computational methods. *J. Mol. Liq.* **2022**, *359*, 119219. [[CrossRef](#)]
52. Palgunadi, J.; Palgunadi, J.; Kang, J.E.; Cheong, M.S.; Kim, H.G.; Lee, H.J.; Kim, H.S. Fluorine-Free Imidazolium-Based Ionic Liquids with a Phosphorous-Containing Anion as Potential CO₂ Absorbents. *Bull. Korean Chem. Soc.* **2009**, *30*, 1749–1754.
53. Li, C.; Feng, S.; Xu, L.; Peng, X.; Liu, W. Solubilities of CO₂, O₂ and N₂ in rocket propellant 5 under low pressure. *Sci. Rep.* **2022**, *12*, 1–10. [[CrossRef](#)] [[PubMed](#)]
54. Li, X.; Liu, X.; Deng, D. Solubilities and Thermodynamic Properties of CO₂ in Four Azole-Based Deep Eutectic Solvents. *J. Chem. Eng. Data* **2018**, *63*, 2091–2096. [[CrossRef](#)]
55. Jalili, A.H.; Shokouhi, M.; Maurer, G.; Zoghi, A.T.; Ahari, J.S.; Forsat, K. Measuring and modelling the absorption and volumetric properties of CO₂ and H₂S in the ionic liquid 1-ethyl-3-methylimidazolium tetrafluoroborate. *J. Chem. Thermodyn.* **2019**, *131*, 544–556. [[CrossRef](#)]
56. Leinweber, A.; Mu, K. Solubility of carbon dioxide, methane, and nitrogen in liquid dibenzyl toluene. *J. Chem. Eng. Data* **2018**, *63*, 3527–3533. [[CrossRef](#)]
57. Losetty, V.; Matheswaran, P.; Wilfred, C.D. Synthesis, thermophysical properties and COSMO-RS study of DBU based protic ionic liquids. *J. Chem. Thermodyn.* **2017**, *105*, 151–158. [[CrossRef](#)]
58. Shahrom, M.S.R.; Wilfred, C.D.; MacFarlane, D.R.; Vijayraghavan, R.; Chong, F.K. Amino acid based poly (ionic liquid) materials for CO₂ capture: Effect of anion. *J. Mol. Liq.* **2019**, *276*, 644–652. [[CrossRef](#)]
59. Khan, H.W.; Elgharrawy, A.A.; Bustam, A.; Moniruzzaman, M. Design and selection of ionic liquids via COSMO for pharmaceuticals and medicine. In *Application of Ionic Liquids in Drug Delivery*; Springer: Singapore, 2021; pp. 137–164.
60. Qin, C.; Gao, H.; Liu, X.; Li, X.; Xie, Y.; Bai, Y.; Nie, Y. The dissolution of human hair using ionic liquids through COSMO-RS prediction and experimental verification. *J. Mol. Liq.* **2022**, *349*, 118094. [[CrossRef](#)]
61. Palomar, J.; Gonzalez-Miquel, M.; Polo, A.; Rodriguez, F. Understanding the Physical Absorption of CO₂ in Ionic Liquids Using the COSMO-RS Method. *Ind. Eng. Chem. Res.* **2011**, *50*, 3452–3463. [[CrossRef](#)]
62. Villarroya, E.; Olea, F.; Araya-López, C.; Merlet, G.; Cabezas, R.; Romero, J.; Quijada-Maldonado, E. COSMO-RS evaluation as a tool for prediction of solvents in dispersive liquid-phase microextraction: Evaluation of conventional solvents and ionic liquids as extractants. *J. Mol. Liq.* **2022**, *354*, 118861. [[CrossRef](#)]
63. Balchandani, S.; Singh, R. COSMO-RS Analysis of CO₂ Solubility in N-Methyldiethanolamine, Sulfolane, and 1-Butyl-3-methylimidazolium Acetate Activated by 2-Methylpiperazine for Postcombustion Carbon Capture. *ACS Omega* **2020**, *6*, 747–761. [[CrossRef](#)]
64. Wojcickowski, J.P.; Abranches, D.O.; Ferreira, A.M.; Mafra, M.R.; Coutinho, J.A. Using COSMO-RS to predict solvatochromic parameters for deep eutectic solvents. *ACS Sustain. Chem. Eng.* **2021**, *9*, 10240–10249. [[CrossRef](#)]
65. Bououden, W.; Benguerba, Y.; Darwish, A.S.; Attoui, A.; Lemaoui, T.; Balsamo, M.; Erto, A.; Alnashef, I.M. Surface adsorption of Crizotinib on carbon and boron nitride nanotubes as Anti-Cancer drug Carriers: COSMO-RS and DFT molecular insights. *Journal of Molecular Liquids. J. Mol. Liq.* **2021**, *338*, 116666. [[CrossRef](#)]
66. Sosa, J.E.; Santiago, R.; Redondo, A.E.; Avila, J.; Lepre, L.F.; Gomes, M.C.; Araújo, J.M.; Palomar, J.; Pereiro, A.B. Design of ionic liquids for fluorinated gas absorption: COSMO-RS selection and solubility experiments. *Environ. Sci. Technol.* **2022**, *56*, 5898–5909. [[CrossRef](#)]
67. Cao, Y.; Wu, Z.; Zhang, Y.; Liu, Y.; Wang, H. Screening of alternative solvent ionic liquids for artemisinin: COSMO-RS prediction and experimental verification. *J. Mol. Liq.* **2021**, *338*, 116778. [[CrossRef](#)]
68. Eckert, F.; Klamt, A. *COSMOtherm*; Release 19.0.1; COSMOlogic GmbH & Co. Kg.: Leverkusen, Germany, 2013.
69. Klamt, A. *COSMO-RS: From Quantum Chemistry to Fluid Phase Thermodynamics and Drug Design*; Elsevier BV: Amsterdam, The Netherlands, 2005.
70. Klamt, A. Conductor-like screening model for real solvents: A new approach to the quantitative calculation of solvation phenomena. *J. Phys. Chem.* **1995**, *99*, 2224–2235. [[CrossRef](#)]
71. Klamt, A.; Jonas, V.; Bürger, T.; Lohrenz, J.C. Refinement and parametrization of COSMO-RS. *J. Phys. Chem A* **1998**, *102*, 5074–5085. [[CrossRef](#)]
72. Liu, X.; Zhou, T.; Zhang, X.; Zhang, S.; Liang, X.; Gani, R.; Kontogeorgis, G.M. Application of COSMO-RS and UNIFAC for ionic liquids based gas separation. *Chem. Eng. Sci.* **2018**, *192*, 816–828. [[CrossRef](#)]
73. Lei, Z.; Yuan, J.; Zhu, J. Solubility of CO₂ in Propanone, 1-Ethyl-3-methylimidazolium Tetrafluoroborate, and Their Mixtures. *J. Chem. Eng. Data* **2010**, *55*, 4190–4194. [[CrossRef](#)]
74. Kim, Y.; Choi, W.Y.; Jang, J.H.; Yoo, K.P.; Lee, C.S. Solubility measurement and prediction of carbon dioxide in ionic liquids. *Fluid Phase Equilib.* **2005**, *228*, 439–445. [[CrossRef](#)]

75. Sistla, Y.S.; Khanna, A. CO₂ absorption studies in amino acid-anion based ionic liquids. *Chem. Eng. J.* **2015**, *273*, 268–276. [[CrossRef](#)]
76. Onofri, S.; Adenusi, H.; Le Donne, A.; Bodo, E. CO₂ Capture in Ionic Liquids Based on Amino Acid Anions With Protic Side Chains: A Computational Assessment of Kinetically Efficient Reaction Mechanisms. *ChemistryOpen* **2020**, *9*, 1153–1160. [[CrossRef](#)] [[PubMed](#)]
77. Shannon, M.S.; Tedstone, J.M.; Danielsen, S.P.; Hindman, M.S.; Irvin, A.C.; Bara, J.E. Free volume as the basis of gas solubility and selectivity in imidazolium-based ionic liquids. *Ind. Eng. Chem. Res.* **2012**, *51*, 5565–5576. [[CrossRef](#)]
78. Greb, L. Lewis superacids: Classifications, candidates, and applications. *Chem. Eur. J.* **2018**, *24*, 17881–17896. [[CrossRef](#)] [[PubMed](#)]
79. Kong, T.; Jiang, Y.; Xiong, Y. Photocatalytic CO₂ conversion: What can we learn from conventional CO x hydrogenation? *Chem. Soc. Rev.* **2020**, *49*, 6579–6591. [[CrossRef](#)] [[PubMed](#)]
80. Klamt, A. COSMO-RS for aqueous solvation and interfaces. *Fluid Phase Equilib* **2016**, *407*, 152–158. [[CrossRef](#)]

Disclaimer/Publisher’s Note: The statements, opinions and data contained in all publications are solely those of the individual author(s) and contributor(s) and not of MDPI and/or the editor(s). MDPI and/or the editor(s) disclaim responsibility for any injury to people or property resulting from any ideas, methods, instructions or products referred to in the content.